# Observation of an Ultrafast Exciton Transport Regime at Early Times in Quantum Dot Solids

**Zhilong Zhang**
University of Cambridge https://orcid.org/0000-0001-9903-4945
**Jooyoung Sung**
University of Cambridge
**Daniel Toolan**
University of Sheffield
**Sanyang Han**
University of Cambridge https://orcid.org/0000-0001-7414-7193
**Michael Weir**
University of Nottingham https://orcid.org/0000-0001-8283-1040
**James Xiao**
University of Cambridge
**Simon Dowland**
University of Cambridge
**Mengxia Liu**
University of Cambridge
**Anthony Ryan**
University of Sheffield
**Richard Jones**
Department of Physics & Astronomy
**Shujuan Huang**
UNSW Australia https://orcid.org/0000-0003-3468-4773
**Akshay Rao** ( ar525@cam.ac.uk )
University of Cambridge https://orcid.org/0000-0003-0320-2962

**Research Article**

**Keywords:** quantum dots, quantum dot solids, ultrafast exciton transport

**Posted Date:** September 15th, 2020

**DOI:** https://doi.org/10.21203/rs.3.rs-75982/v1

**Version of Record:** A version of this preprint was published at Nature Materials on March 7th, 2022. See the published version at https://doi.org/10.1038/s41563-022-01204-6.

# Observation of an Ultrafast Exciton Transport Regime at Early Times in Quantum Dot Solids

Zhilong Zhang[1], Jooyoung Sung[1*], Daniel T. W. Toolan[2], Sanyang Han[1], Michael P. Weir[3], James Xiao[1], Simon Dowland[1], Mengxia Liu[1], Anthony J. Ryan[2], Richard A. L. Jones[3], Shujuan Huang[4] and Akshay Rao[1*]

[1]Cavendish Laboratory, J.J. Thomson Avenue, University of Cambridge, Cambridge CB3 OHE, United Kingdom.

[2]Department of Chemistry, The University of Sheffield, Sheffield S3 7HF, United Kingdom

[3]Department of Physics and Astronomy, The University of Sheffield, Sheffield S3 7RH, United Kingdom

[4]Australian Centre for Advanced Photovoltaics (ACAP), School of Photovoltaic and Renewable and Engineering, University of New South Wales, Sydney, 2052 Australia

*email: ar525@cam.ac.uk, js2377@cam.ac.uk

**Understanding and engineering exciton transport in quantum dot (QD) solids is both of fundamental interest and crucial to their broad applications in devices[1-6]. Till date, studies of exciton transport in QD solids on pico/nano-second timescales have led to the conclusion that closer packing of QDs enables faster exciton transport, while energetic/structural heterogeneity leads to reduction of exciton diffusivity over time[7,8]. Here we study PbS QD solids using transient absorption microscopy with 13 femtoseconds time resolution and 10 nm spatial precision. We find exciton diffusivities in the range of ~$10^2$ $cm^2$ $s^{-1}$ within the first few hundred femtoseconds after photoexcitation, followed by the transition to a slower transport regime with diffusivities in the range $10^{-1}$ to 1 $cm^2$ $s^{-1}$. Counterintuitively, the initial diffusivity is higher and the time before the transition to the slower transport phase is longer in QD solids with longer ligand lengths. This suggests a transition from early time transport of delocalized excitons to later time hopping based transport of localized excitons, where QD packing density and heterogeneity accelerate the localization process. Our results reveal a new regime for exciton transport in QD solids and provide design rules to engineer desired transport properties in these systems on a range of timescales.**

Colloidal QDs have attracted great interest for fundamental studies of exciton and charge dynamics in semiconductor nanostructures, as well as for their applications in various devices including photodetectors[3], light emitting diodes (LEDs)[4], photovoltaics[5,6] and field effect transistors (FETs)[9]. One of the fundamental physical processes underlying the function of these devices is exciton transport in the QD active layer, which is believed to be determined via the assembly of QDs within the film[1-4,10,11]. The requirement for exciton transport however differs between different applications, for example, a photovoltaic cell requires fast exciton transport to the charge-separating interfaces[5,6], whereas in a LED this can lead to quenching of

photoluminescence[1,4]. A comprehensive understanding of exciton transport physics in QD solids is therefore needed, with the eventual aim of controlling these transport properties in order to optimize device performance.

In comparison to the parallel issue of charge transport, the understanding of exciton transport in QD solids is less developed. This partly arises due to limitations of experimental techniques. While FETs and Hall measurements under steady-state conditions provide a wealth of information on charge transport[1,2,9], excitons cannot be easily probed electrically in ensemble measurements. Coupled with their short-lifetime (<5 μs normally) and short diffusion lengths (in comparison to charges), this limits studies of exciton transport to quenching or optical microscopy measurements. Time-resolved microscopy has been particularly powerful in probing exciton transport, especially at linking transport to underlying disorder in the materials and probing time-dependent diffusion of excitons[7,8,12-14]. The general consensus that emerges from these studies is that closer packing of QDs enables faster exciton transport, while energetic/structural heterogeneity leads to reduction of exciton diffusivity over time[7,8]. These conclusions together with the extracted diffusivities (ranging from $10^{-3}$ to $10^{-2}$ $cm^2$ $s^{-1}$) fit well within the picture of Förster resonance energy transfer (FRET) dominated hopping of excitons within a disordered energy landscape[14]. However, due to experimental limitations these studies have probed exciton transport in QD solids on pico/nano-second timescales following photoexcitation. As exciton behaviour can be time-dependent, those conclusions can also be limited by the timescale measured. One important part of the picture is therefore still missing - exciton transport at early times (femtosecond timescale) following photoexcitation.

Here we probe this unexplored regime of exciton transport in QD solids by directly imaging exciton motion on femtosecond (fs) timescale following generation. Surprisingly, we discovered that excitons first undergo very fast transport (diffusivity range of ~$10^2$ $cm^2$ $s^{-1}$) within ~300 fs after photoexcitation and then switch into a much slower transport regime (~$10^{-1}$ to 1 $cm^2$ $s^{-1}$). Intriguingly, reducing the interdot distance in the QD solids only enhances transport in the slower regime, while it unexpectedly diminishes the initial fast regime. We suggest that both QD packing density and heterogeneity have significant impacts on these transport regimes and the transition between them.

To directly monitor exciton transport at early times, we performed femtosecond transient absorption microscopy (fs-TAM) measurement on the QD films (Fig. 1a). A full description of the instrument is provided in Supplementary Methods. Briefly, a near diffraction-limited pump beam (an effective width $\sigma$ of 107 ± 7.5 nm) with transform-limited pulse duration (9.2 fs) is delivered onto the QD film, generating a Gaussian-shaped exciton density instantaneously. The spatial evolution of exciton distribution is recorded by imaging it with a loosely focused (a width of 6.4 μm) and transform-limited (6.8 fs) probe pulse at a series of variable time delays between pump and probe pulses. It should be noted that although spatial resolution is still limited by diffraction, by comparing subsequent TAM images it is possible to distinguish the changes in the shape of the distribution as small as 10 nm (Supplementary Methods)[15,16]. Thus the fs-TAM methodology allows us to study exciton motion with at least 13 fs temporal resolution and 10 nm spatial precision.

Lead sulfide (PbS) QDs (bandgap of 1.68 eV as-synthesized) were chosen as the material platform in this work, as they are among the most intensively studied materials for QD-based

devices due to the highly tuneable band gap, relatively good stability, carrier transport and photoluminescence[2,4,5]. A series of PbS QD solid-state films with systematic variation in the interdot spacing was prepared. This was achieved by solution-phase pre-exchange of the native oleic acid (OA) capping ligands arising from the synthesis to those with shorter carbon chains (Fig. 1b), namely dodecanoic acid (12C), octanoic acid (8C), hexanoic acid (6C) and butyric acid (4C) before film fabrication by spin-coating (Supplementary Methods). Hereafter, the QD films are denoted as the corresponding ligands. The samples were encapsulated prior to optical characterizations. Both the PL and excitonic features of the absorption spectra were maintained, indicating successful ligand exchange without noticeable aggregation (Supplementary Figs. 1-3).

Conventional ensemble level transient absorption (TA) features of the QD films were explored before the fs-TAM measurements (Supplementary Figs. 4-8). As shown in Fig. 1c, gradual red-shifts of the photo-bleaching peaks were observed (from 730 nm of OA) in the TA spectra of the films with reducing ligand lengths, which is consistent with shorter interdot distance and stronger coupling[7,17]. It is noticeable that there was little signal decay within the measurement time window of fs-TAM (kinetics in Supplementary Fig. 9), suggesting very little recombination on these early timescales and hence this is unlikely to affect the transport measurements.

The fs-TAM images of each film were recorded at the probe wavelength corresponding to the photo-bleaching peaks (with a bandwidth of 10 nm, shaded areas shown in Figure 1c). Representative fs-TAM images obtained from OA at early time are shown in Fig. 1d, while data sets for the other samples can be found in Supplementary Figs. 10-13. The series of fs-

TAM images clearly show spatial expansion of exciton distribution in the QD film. Since the initially generated exciton distribution resembles the diffraction-limit pump beam and the spatial expansion occurs isotropically, we fitted the fs-TAM images with an isotropic two-dimensional Gaussian function and extracted the corresponding width, $\sigma$, as shown in Fig. 1e (and Supplementary Fig. 14). Near time-zero, the initially created exciton distribution gives a width of 172 ± 8 nm, which is similar to the distribution width (180 nm) calculated by convoluting diffraction-limited pump and probe beams[15]. By 260 fs this distribution expands to 224 ± 8 nm, clearly indicating exciton transport at early times in the QD film.

To quantitatively compare the transport dynamics in QD films, we employ the widely adopted approach of quantifying the spread of spatial exciton distribution by monitoring the change in profile variance, i.e. the mean squared displacement (MSD = $\sigma_t^2 - \sigma_0^2$) model[7,12,15,16]. For quantitative comparison, the MSD profiles of the films over time are plotted in Fig. 2a. Interestingly, two distinct transport regimes seem to exist in the MSD profiles: a very fast initial expansion of the exciton distribution within the first ~300 fs upon photoexcitation, followed by a much slower expansion (up to 4 ps time window of measurement). To test whether it is a two-step diffusion process or an anomalous diffusion process, we fitted the MSD evolution with the power law equation as MSD = $2Dt^{\alpha}$, where $D$ is the diffusivity and $\alpha$ is the diffusion exponent[7,14,15,18]. We noticed that the MSD profiles cannot be fitted by a single power law equation, due to the abrupt transition from the fast to the slow expansion stage (Supplementary Discussion 1 and Supplementary Fig. 15). Instead, the profiles can be well-fitted within separated time ranges for all samples. The fitting results of OA is shown in Fig. 2b as an example. Within the range of $t_0 < t < t_{fast}$, the dynamics can be well described by a power law equation where $\alpha = 1$, signifying that the initial exciton transport is diffusive[7,8,14,15,18]. The corresponding diffusivity ($D_{fast}$) can therefore be extracted from the slope of the fitted line.

Similarly, for $t > t_{slow}$ the MSD profile can also be described by diffusive motion ($\alpha = 1$) with a much smaller diffusivity ($D_{slow}$). A transition stage (where $t_{fast} < t < t_{slow}$) also exists between the fast and slow diffusive stages. Alternatively, the slow diffusive region can be described by a subdiffusive motion where $\alpha < 1$ (Supplementary Table. 2) by including the transition stage (blue dotted curve, Fig. 2b). We note here that whether we take the description of diffusive or subdiffusive motion for the later slow transport the conclusion is consistent with that discussed below (Supplementary Discussion 2).

Interestingly, the extracted diffusivities from the fast and slow transport stages have opposite response to the reduction of ligand length in the series of QD films (Fig. 2c). It has been generally believed that reducing the ligand length can lead to shorter interdot distance, hence improved QD coupling and transport[1-3]. Consistent with this general perception, the obtained diffusivities in the slow regime increases with shorter ligands in the QD films ($D_{slow}$, red dots, Fig. 2c), apart from 4C. The values of $D_{slow}$ from 0.6 to 1.5 $cm^2\ s^{-1}$ were also comparable with exciton diffusivities reported in other QD systems[7,8], suggesting the slow stage is likely governed by classical FRET hopping regime[14].

Intriguingly, the extracted diffusivities from the fast region ($D_{fast}$) decrease with reducing ligand length, opposite to general perception of QD solids and the slow transport regime. The highest $D_{fast}$ was obtained from OA (with the longest ligand), followed by 12C, 8C and 6C (black dots, Fig. 2c). 4C was again an exception, while its $D_{fast}$ was higher than those with the medium-length ligands, however still lower than that of OA. Moreover, the values of the extracted $D_{fast}$ are within the range from 95 to 280 $cm^2\ s^{-1}$, which is three to four orders of magnitude higher than those from $D_{slow}$. We emphasize that such an early-time process of

exciton transport in QD solids is revealed here experimentally for the first time. It has been well demonstrated that the exciton diffusivity of disordered systems such as QD and organic semiconductor solids decrease over time[7,12,13,18]. Therefore higher diffusivities in such an early-time range (< 300 fs) can be expected. Nevertheless, the observed $D_{fast}$ values are obviously too high to be described by classical hopping in QD solids, implying the fast regime is likely governed by a different mechanism. Interestingly, the estimated $t_{fast}$ also shows the same behaviour as $D_{fast}$ (black dots, Fig. 2d), indicating that films with longer ligands can sustain the initial fast transport for longer time. Similarly, the trend in $t_{slow}$ also suggests longer ligands postpone the transition from the fast to the slow stage (red dots, Fig. 2d).

Important questions then arise as to what are the underlying mechanisms that dictate the two distinct transport regimes and why they have reversed trends of diffusivities when the ligand length was reduced. To further elucidate these, we looked into the quality and actual packing of the QD solids with different ligands. We first compared the PLQY of the QD solids with those of the corresponding QD solutions (Fig. 3a). The PLQY of the QDs in solution were all around 35 ~ 40%, indicating they had similar level of surface defects and aggregation. In contrast, the drop of PLQY when cast into films was more significant with shorter ligands, consistent with the expectation of better QD coupling and concomitant PL quenching[1,19]. We then performed grazing incidence small angle x-ray scattering (GISAXS) to reveal the actual interdot distance and packing heterogeneity (Fig. 3b and Supplementary Fig. 16). We found the average interdot distance (core-to-core) decreased from ~37.2 Å for OA to ~31.5 Å for both 8C and 6C, whilst 4C maintained an unexpectedly large separation of ~35.5 Å (red dots, Fig. 3c). The QD packing disorder (FWHM of the peaks) however gradually increased with shorter ligands (black dots, Fig. 3c). We therefore attribute the unexpectedly large interdot distance of 4C to its high packing heterogeneity (Supplementary Discussion 3), which may have also

caused 4C to be an exception to the trend of diffusivities from Fig. 2c. We then correlate the diffusivities from Fig. 2c with the actual interdot distance of the films, and again confirm that $D_{slow}$ increases with reduction of the actual interdot distance, while $D_{fast}$ has the opposite trend (Fig. 3d).

Both the trend and values of $D_{slow}$ suggest that the slow regime is governed by a classical hopping mechanism of localized excitons. In contrast, the high values of $D_{fast}$ and its trend with interdot distance are highly unusual. This phase of transport is still diffusive in nature (as $\alpha$ = 1), which would seem to rule out ballistic or coherent exciton motion[14,20,21]. One possible explanation is the transport of delocalized rather than localized excitons at early times[10,22] (also see Supplementary Discussion 4). Theoretical prediction suggests that delocalized excitons can transfer to sites that are spatially far away due to the enhanced net transition dipole moment from superposition of individual QD wavefunctions, leading to much higher diffusivity, via 'supertransfer' mechanism[23,24]. Further experimental and theoretical investigations are called for to investigate this phenomena at early times.

The transition from the fast to the much slower transport regime observed from our results can then be explained as the switch to the diffusion of localized excitons from the early time delocalized transport. We note the transition time between the two regimes is shorter in QD films with higher level of packing disorder ($t_{trans} = t_{slow} - t_{fast}$, Fig. 3e), although it is difficult to decouple this from the effect of shorter interdot distance. Nevertheless, despite the fact that 4C has an average interdot distance between those of OA and 8C/6C, it has the shortest $t_{trans}$ among all (Fig. 3e), clearly suggesting packing disorder accelerates the transition from the fast to the slow transport regime.

The important remaining question is why the initial fast transport is less efficient in QD solids when decreasing interdot distance (Fig. 3d). Here, we suggest that one aspect of disorder that has been largely overlooked may cause this – the QD packing density that increases with reduction of interdot distance (Supplementary Fig. 17). Conventional sources of disorder in QD solids include size polydispersity, surface defect states and packing heterogeneity[5,7,9]. But assuming the same polydispersity and defect level per QD, increasing the packing density would unavoidably increase the number of QDs contributing to disorder within the same volume. This would introduce more scattering sites into the transport path of a delocalized exciton initially generated and accelerate the transition to the localized transport regime. Similar observations have been made in carrier transport of organic semiconductors such as rubrene thin films, where the highest mobility was found in a packing direction with larger intermolecular distance[25,26]. We speculate that this may be origin of the less efficient fast transport of delocalized excitons and rapid transition to slow regime in QD solids with shorter interdot distance.

With the above results, we depict the exciton transport profile in the early timescale as shown in Fig. 4. Immediately after photoexcitation, delocalized excitons are generated in the QD solids. They then diffuse quickly in the solid (fast transport regime), and during this stage when an exciton encounters a shallow trap state it may even have sufficient energy to escape as it is still undergoing a cooling process (as shown by TA kinetics in Supplementary Fig. 9)[15]. In the case of a QD solid with larger (but still closely-packed) interdot distance and/or homogeneous packing (Fig. 4a), a low level of disorder allows the fast transport to be faster and sustained for longer. However, when an exciton is eventually localized, the transport mechanism switches

to a hopping (slow) regime that is much less efficient with a longer QD separation. In the case of a QD solid with shorter interdot distance (Fig. 4b), the higher packing density can introduce more QDs as the sources of disorder/scattering sites for a delocalized exciton. A faster localization process occurs and limits the fast transport rate and duration. High packing heterogeneity can further accelerate the localization process. Once the exciton is localized, however it can still transport through the QDs relatively efficient by hopping due to the short interdot separation, as one would normally expect in longer timescales.

In summary, our work has revealed the early time exciton dynamics in QD solids. We observed the transition from a very fast to a slow regime over time, which we suggest to be related to the localization process of delocalized excitons. While the slow regime was comparable with classical hopping, the fast regime demonstrated diffusivities of three to four orders of magnitudes faster than those of the slow regime, as well as other reports on exciton transport on longer timescales[7,8]. Counterintuitively, the early-time regime was faster and sustained for longer in QD solids with relatively larger interdot distance, opposite to the classical longer-time hopping transport process. We attribute this to disorders arising from higher QD packing density (hence disorder density) and structural heterogeneity that accelerate exciton localization. This study sheds light on the factors that dictate exciton transport in QD solids on fs timescales and provides design rules to engineer QD solids to tailor the desired transport properties in these systems on a range of timescales.

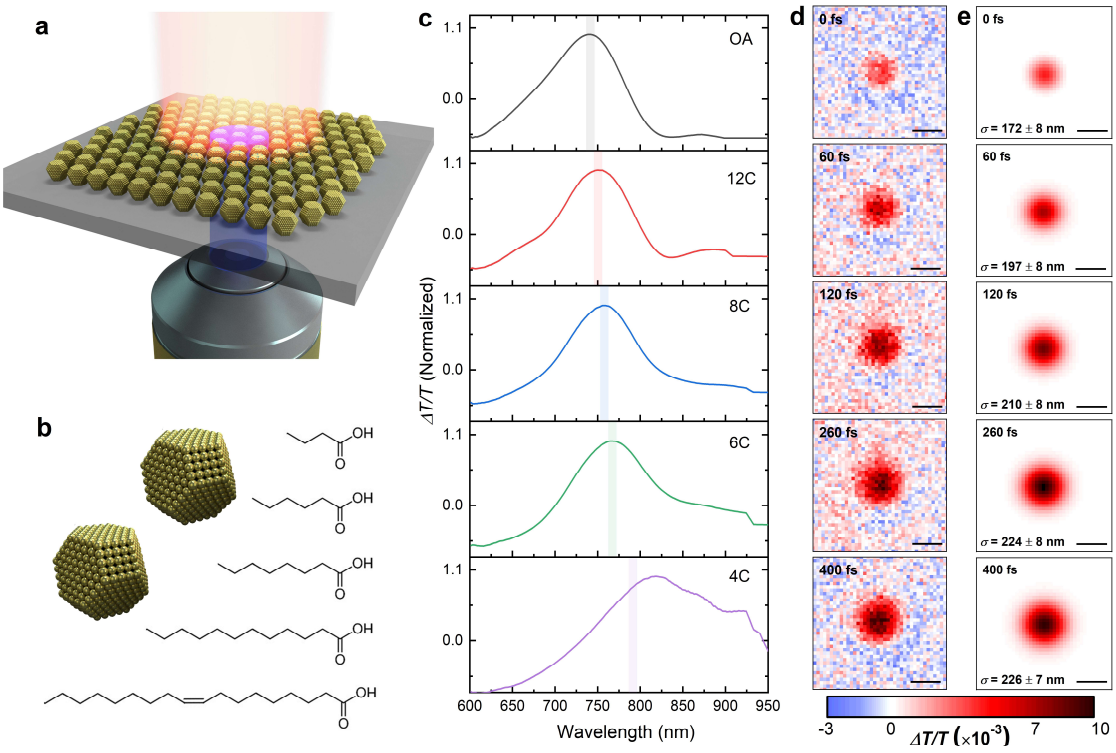


**Fig. 1 The fs-TAM measurement of QD thin films with different capping ligands as discussed in this work. a**, Schematic representation of the fs-TAM measurement. A near diffraction-limited ($\sigma$ of 107 ± 7.5 nm) and transform-limited (9.2 fs, 580 nm) pump beam is delivered onto the QD film (blue beam), together with a counter-propagating loosely focused ($\sigma$ of 6.4 μm) and transform-limited (6.8 fs) probe pulse (orange beam). Note that the actual samples are thicker films containing multiple layers of QDs with total thickness about 200 nm. **b**, The interdot distance of the films were modified by the selection of surface ligands. The ligand exchange was performed to replace the original OA ligands to 12C, 8C, 6C or 4C ligands in solution-phase prior to film fabrication. **c**, Normalized TA spectra of the QD films with different ligands at 1 ps pump-probe time delay. Gradual red-shifts of the peaks were observed with shorter ligands. The fs-TAM data was taken near the corresponding positive $\Delta T/T$ photobleaching peaks with a bandwidth of 10 nm (shaded area). **d**, Representative fs-TAM images of OA at 0, 60, 120, 260 and 400 fs pump-probe delay, respectively. A spectral bandwidth of 10 nm was achieved by using a bandpass filter (730 nm) in the imaging path. **e**,

The corresponding exciton distribution images retrieved by fits with isotropic two-dimensional Gaussian functions. The $\sigma$ values represent the width of exciton distribution at the corresponding time delay. Clear expansion of exciton distribution over time can be observed. Scale bars, 500 nm.

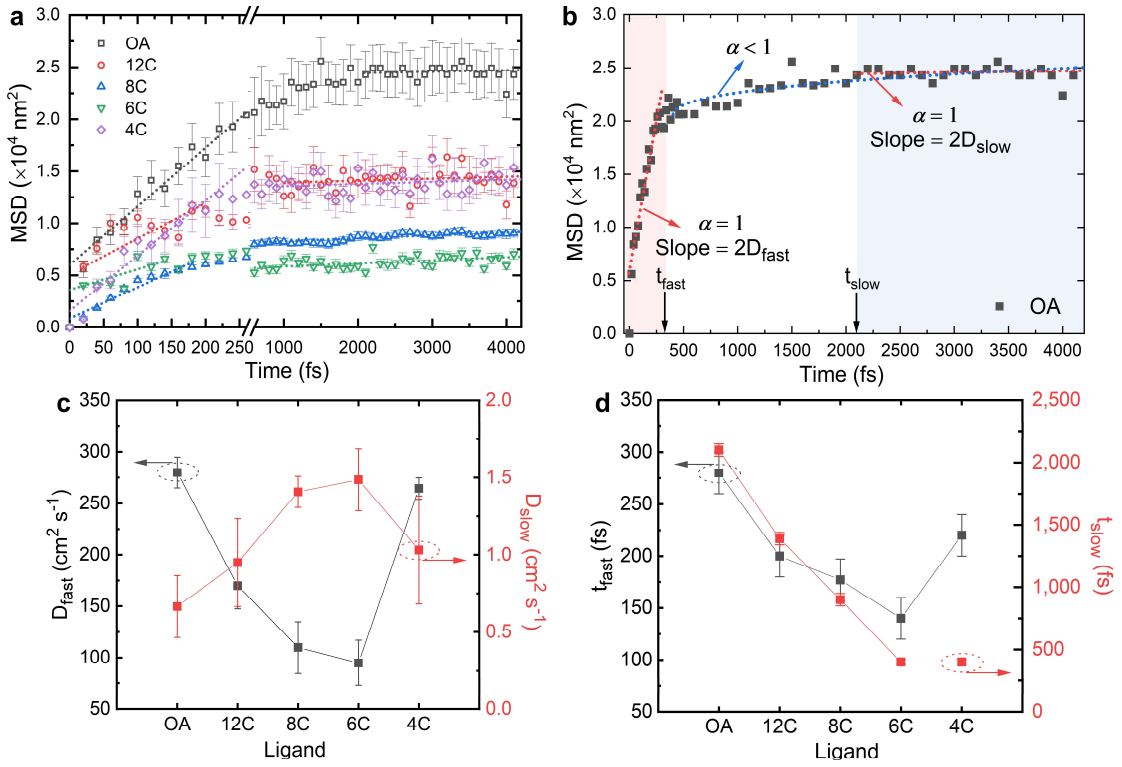


287

288 **Fig. 2 Quantitative fs-TAM measurement results of the series of QD thin films. a**, Time
289 evolution of the MSD = $\sigma_t^2 - \sigma_0^2$ profile, while $\sigma_0^2$ represents the width of the spatial exciton
290 distribution near zero pump-probe delay. The dotted lines are the fits within the respective
291 time range based on the power law of MSD = $2Dt^{\alpha}$, where $\alpha = 1$. **b**, The fitted curves and
292 resultants parameters extracted for a representative QD film, OA as an example. The MSD
293 profile within the time range of $0 < t < t_{fast}$ and that of $t > t_{slow}$ can be well described by the
294 diffusive motion such that $\alpha = 1$ from the power law equation (red dotted line), where the
295 diffusivities of $D_{fast}$ and $D_{slow}$ can be extracted from the slope of the corresponding fitted
296 lines. The MSD profile after $t_{fast}$ can also be described by a subdiffusive motion (blue dotted
297 line, $\alpha < 1$), while conclusions from the two fitting methods are consistent (Supplementary
298 Discussion 2). **c**, The extracted diffusivities of the initial fast transport regime ($D_{fast}$) and the
299 slow regime ($D_{slow}$) of the series of QD films. The two transport regimes show opposite

response to the variation of ligands. **d**, The estimated time duration of the initial fast stage ($t_{fast}$) and the time taken (from 0 fs) for the excitons to enter the slow transport regime ($t_{slow}$).

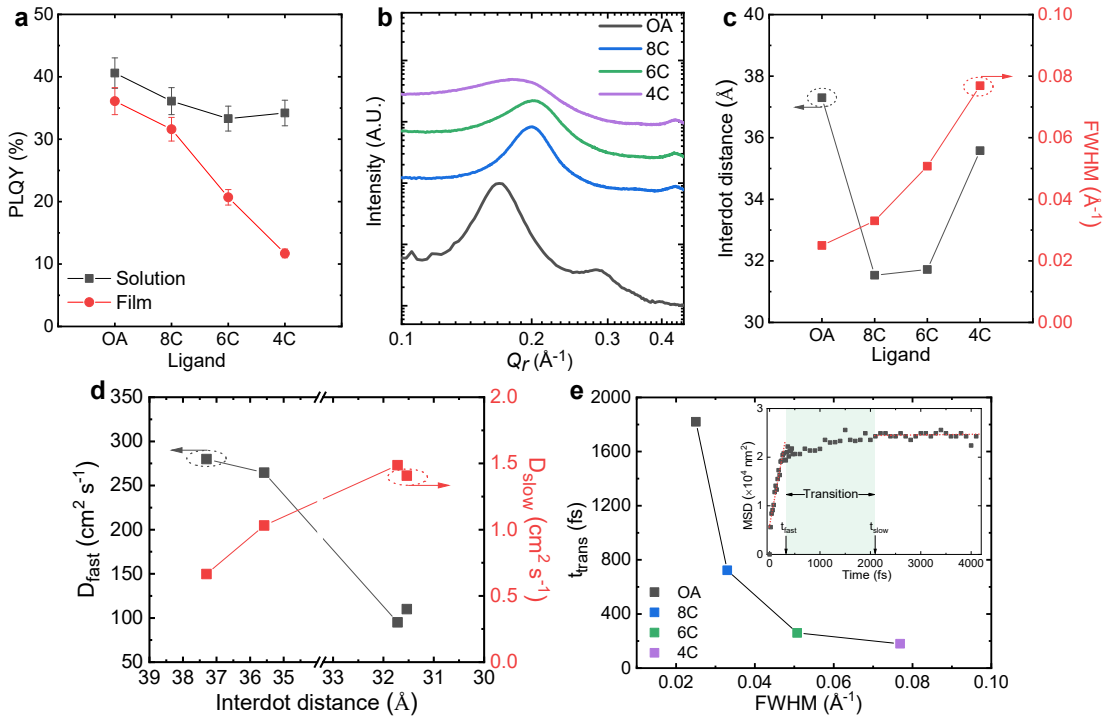


315

316 **Fig. 3 Quality and structural information of the QDs and films with different ligands**
317 **and correlation to the fs-TAM results. a**, PLQY of the QDs in both solution- and solid-
318 state with different ligands. A more significant quenching in the PLQY can be observed from
319 films with shorter ligands. No chemical or thermal treatment was applied to the films,
320 indicating that the quenching of PLQY arises from improved QD coupling due to closer
321 interdot distance. **b**, Radially integrated GISAXS intensities of QD solids (normalized).
322 Lower $Q_r$ value of the 1st order scattering peaks indicates larger average separation between
323 the QDs, while the peak width indicates discrepancy of the separation. **c**, The fitted interdot
324 distance and FWHM of the 1st order scattering peaks from **b**. We ascribe the FWHM to a
325 relative deviation in the core-to-core spacing of the QDs and hence level of packing disorder
326 in the samples. **d**, Correlation between the actual interdot distance (core-to-core) with the
327 diffusivities of the fast and slow regimes. The $D_{fast}$ decreases with reducing interdot distance
328 while $D_{slow}$ clearly shows an opposite trend. **e**, Correlation between the transition time ($t_{trans}$ =
329 $t_{slow} - t_{fast}$, inset) with the FWHM (level of packing disorder) of the 1st order scattering peaks

in **b**. The decreasing $t_{trans}$ with increasing FWHM indicates higher level of disorder leads to faster transition from the fast to the slow regime.

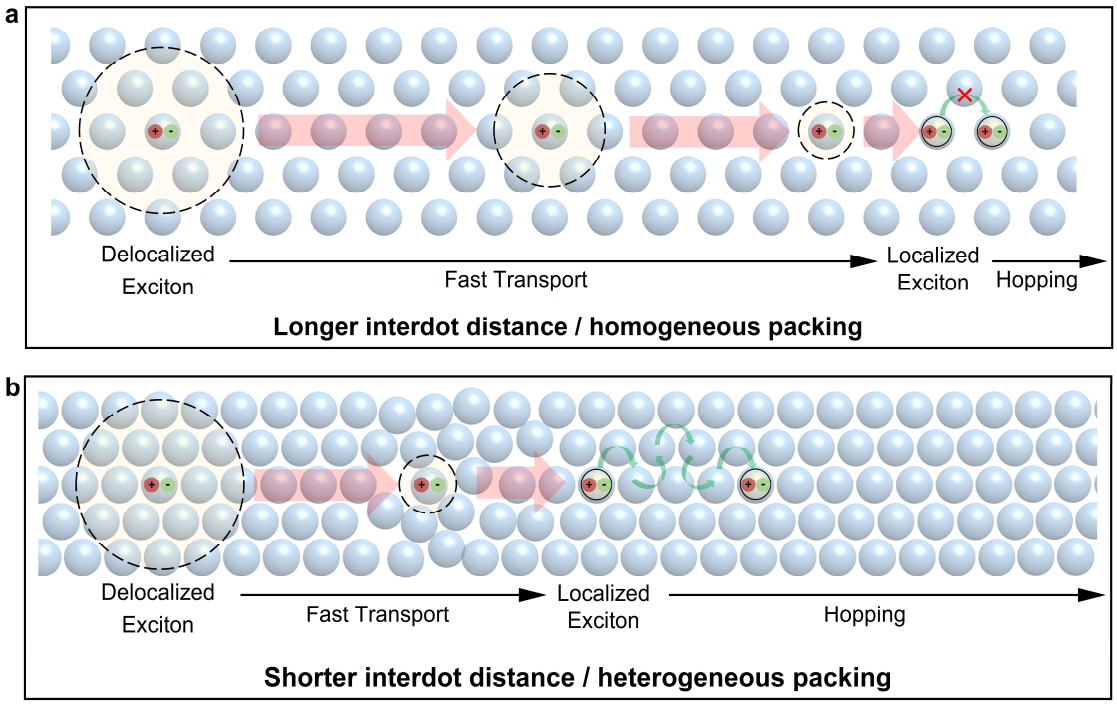


346

347 **Fig. 4 Schematic of early time exciton transport in QD solids. a**, The case of QD solids
348 with relatively long (but still closely-packed) interdot distance and/or homogeneous packing.
349 The photogenerated exciton initially delocalizes over multiple QDs and diffuses through the
350 QD solid rapidly. The low QD packing density and lack of disorder allows the transport to be
351 faster and sustained longer. As disorders still exist the exciton would eventually be localized,
352 and after the exciton hopping process is inefficient due to the long interdot distance. **b**, The
353 case of QD solids with shorter interdot distance and/or heterogeneous packing. Due to high
354 QD packing density and the existence of packing disorder, the delocalized exciton diffuses
355 relatively slowly and can be localized much earlier. However, after localization the exciton
356 can keep moving among QDs through hopping due to the shorter interdot distance.

357

358

359

## References


1. Kagan, C. R., Lifshitz, E., Sargent, E. H. & Talapin, D. V. Building devices from colloidal quantum dots. *Science* **353,** aac5523. (2016)
2. Kagan, C. R. & Murray, C. B. Charge transport in strongly coupled quantum dot solids. *Nat. Nanotechnol.* **10,** 1013-1026. (2015)
3. Lee, J. S., Kovalenko, M. V., Huang, J., Chung, D. S. & Talapin, D. V. Band-like transport, high electron mobility and high photoconductivity in all-inorganic nanocrystal arrays. *Nat. Nanotechnol.* **6,** 348-352. (2011)
4. Sun, L., Choi, J. J., Stachnik, D., Bartnik, A. C., Hyun, B. R., Malliaras, G. G.*, et al.* Bright infrared quantum-dot light-emitting diodes through inter-dot spacing control. *Nat. Nanotechnol.* **7,** 369-373. (2012)
5. Liu, M., Voznyy, O., Sabatini, R., Garcia de Arquer, F. P., Munir, R., Balawi, A. H.*, et al.* Hybrid organic-inorganic inks flatten the energy landscape in colloidal quantum dot solids. *Nat. Mater.* **16,** 258-263. (2017)
6. Chuang, C. H., Brown, P. R., Bulovic, V. & Bawendi, M. G. Improved performance and stability in quantum dot solar cells through band alignment engineering. *Nat. Mater.* **13,** 796-801. (2014)
7. Akselrod, G. M., Prins, F., Poulikakos, L. V., Lee, E. M., Weidman, M. C., Mork, A. J.*, et al.* Subdiffusive exciton transport in quantum dot solids. *Nano Lett.* **14,** 3556-3562. (2014)
8. Yoon, S. J., Guo, Z., Dos Santos Claro, P. C., Shevchenko, E. V. & Huang, L. Direct imaging of long-range exciton transport in quantum dot superlattices by ultrafast microscopy. *ACS Nano* **10,** 7208-7215. (2016)
9. Lan, X., Chen, M., Hudson, M. H., Kamysbayev, V., Wang, Y., Guyot-Sionnest, P.*, et al.* Quantum dot solids showing state-resolved band-like transport. *Nat. Mater.* **19,** 323-329. (2020)
10. Crisp, R. W., Schrauben, J. N., Beard, M. C., Luther, J. M. & Johnson, J. C. Coherent exciton delocalization in strongly coupled quantum dot arrays. *Nano Lett.* **13,** 4862-4869. (2013)
11. Choi, J. H., Fafarman, A. T., Oh, S. J., Ko, D. K., Kim, D. K., Diroll, B. T.*, et al.* Bandlike transport in strongly coupled and doped quantum dot solids: a route to high-performance thin-film electronics. *Nano Lett.* **12,** 2631-2638. (2012)
12. Akselrod, G. M., Deotare, P. B., Thompson, N. J., Lee, J., Tisdale, W. A., Baldo, M. A.*, et al.* Visualization of exciton transport in ordered and disordered molecular solids. *Nat. Commun.* **5,** 3646. (2014)
13. Zhu, T., Wan, Y., Guo, Z., Johnson, J. & Huang, L. Two birds with one stone: Tailoring singlet fission for both triplet yield and exciton diffusion length. *Adv. Mater.* **28,** 7539-7547. (2016)
14. Ginsberg, N. S. & Tisdale, W. A. Spatially resolved photogenerated exciton and charge transport in emerging semiconductors. *Annu. Rev. Phys. Chem.* **71,** 1-30. (2020)
15. Sung, J., Schnedermann, C., Ni, L., Sadhanala, A., Chen, R. Y. S., Cho, C.*, et al.* Long-range ballistic propagation of carriers in methylammonium lead iodide perovskite thin films. *Nat. Phys.* **16,** 171-176. (2019)
16. Guo, Z., Manser, J. S., Wan, Y., Kamat, P. V. & Huang, L. Spatial and temporal imaging of long-range charge transport in perovskite thin films by ultrafast microscopy. *Nat. Commun.* **6,** 7471. (2015)

17. Choi, J. J., Luria, J., Hyun, B. R., Bartnik, A. C., Sun, L., Lim, Y. F.*, et al.* Photogenerated exciton dissociation in highly coupled lead salt nanocrystal assemblies. *Nano Lett.* **10,** 1805-1811. (2010)
18. Schnedermann, C., Sung, J., Pandya, R., Verma, S. D., Chen, R. Y. S., Gauriot, N.*, et al.* Ultrafast tracking of exciton and charge carrier transport in optoelectronic materials on the nanometer scale. *J. Phys. Chem. Lett.* **10,** 6727-6733. (2019)
19. Zhang, J., Tolentino, J., Smith, E. R., Zhang, J., Beard, M. C., Nozik, A. J.*, et al.* Carrier transport in PbS and PbSe QD films measured by photoluminescence quenching. *J. Phys. Chem. C* **118,** 16228-16235. (2014)
20. Contreras-Pulido, L. D. & Bruderer, M. Coherent and incoherent charge transport in linear triple quantum dots. *J. Phys. Condens Matter.* **29,** 185301. (2017)
21. Barford, W. & Duffy, C. D. P. Role of quantum coherence and energetic disorder in exciton transport in polymer films. *Phys. Rev. B* **74,** 075207. (2006)
22. Cohen, E., Gdor, I., Romero, E., Yochelis, S., van Grondelle, R. & Paltiel, Y. Achieving exciton delocalization in quantum dot aggregates using organic linker molecules. *J. Phys. Chem. Lett.* **8,** 1014-1018. (2017)
23. Lee, E. M. Y., Tisdale, W. A. & Willard, A. P. Perspective: Nonequilibrium dynamics of localized and delocalized excitons in colloidal quantum dot solids. *J. Vac. Sci. Technol. A* **36,** 068501. (2018)
24. Sharma, A., Zhang, L., Tollerud, J. O., Dong, M., Zhu, Y., Halbich, R.*, et al.* Supertransport of excitons in atomically thin organic semiconductors at the 2D quantum limit. *Light Sci. Appl.* **9,** 116. (2020)
25. Fratini, S., Nikolka, M., Salleo, A., Schweicher, G. & Sirringhaus, H. Charge transport in high-mobility conjugated polymers and molecular semiconductors. *Nat. Mater.* **19,** 491-502. (2020)
26. Schweicher, G., D'Avino, G., Ruggiero, M. T., Harkin, D. J., Broch, K., Venkateshvaran, D.*, et al.* Chasing the "killer" phonon mode for the rational design of low-disorder, high-mobility molecular semiconductors. *Adv. Mater.* **31,** e1902407. (2019)

## Acknowledgement

This work has received funding from the European Research Council (ERC) under the European Union's Horizon 2020 research and innovation programme (grant agreement number 758826). Z. Z. acknowledges funding from the European Union's Horizon 2020 research and innovation programme under the Marie Skłodowska-Curie Actions grant (No. 842271 – TRITON project). D. T. W. T., M. P. W., A. J. R. and R. A. L. J. acknowledge support from the Engineering and Physical Sciences Research Council (UK) via grant EP/P027814/1. We thank Dr. David Paleček for the assistance with the TA spectroscopy

measurements, and Dr. Christoph Schnedermann for the useful discussion on transport dynamics.

## Author contributions

Z.Z., J.S. and A.R. conceived the project, performed the sample synthesis and fabrication, fs-TAM and other optical measurements, and wrote the paper. D.T.W.T., M.P.W., A.J.R. and R.A.L.J. supported and performed the GISAXS measurements and analysis. SY.H and M.L. provided input into the sample preparation. J.X. conducted electron microscopy measurements. S.D. contributed to PLQY measurement setups. SJ.H. provided input to the design of experiments and discussion of results.

## Additional information

Supplementary information is available in the online version of the paper. Correspondence and requests for materials should be addressed to A.R.

## Competing financial interests

The authors declare no competing financial interests.

# Figures

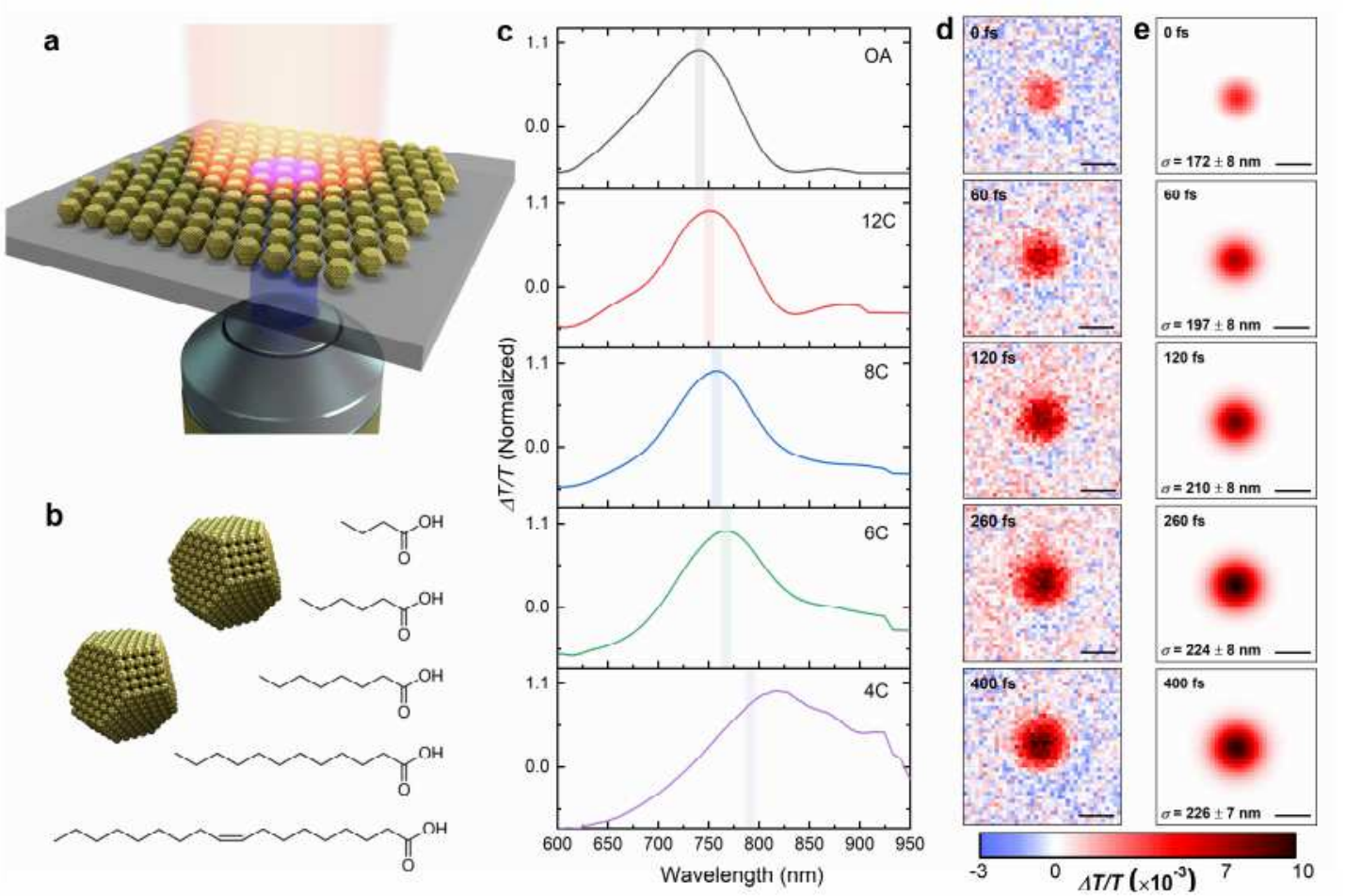


**Figure 1**

The fs-TAM measurement of QD thin films with different capping ligands as discussed in this work. a, Schematic representation of the fs-TAM measurement. A near diffraction-limited (σ of 107 ± 7.5 nm) and transform-limited (9.2 fs, 580 nm) pump beam is delivered onto the QD film (blue beam), together with a counter-propagating loosely focused (σ of 6.4 μm) and transform-limited (6.8 fs) probe pulse (orange beam). Note that the actual samples are thicker films containing multiple layers of QDs with total thickness about 200 nm. b, The interdot distance of the films were modified by the selection of surface ligands. The ligand exchange was performed to replace the original OA ligands to 12C, 8C, 6C or 4C ligands in solution-phase prior to film fabrication. c, Normalized TA spectra of the QD films with different ligands at 1 ps pump-probe time delay. Gradual red-shifts of the peaks were observed with shorter ligands. The fs-TAM data was taken near the corresponding positive ΔT/T photobleaching peaks with a bandwidth of 10 nm (shaded area). d, Representative fs- TAM images of OA at 0, 60, 120, 260 and 400 fs pump-probe delay, respectively. A spectral bandwidth of 10 nm was achieved by using a bandpass filter (730 nm) in the imaging path. e, The corresponding exciton distribution images retrieved by fits with isotropic two- dimensional Gaussian functions. The σ values represent the width of exciton distribution at

the corresponding time delay. Clear expansion of exciton distribution over time can be observed. Scale bars, 500 nm.

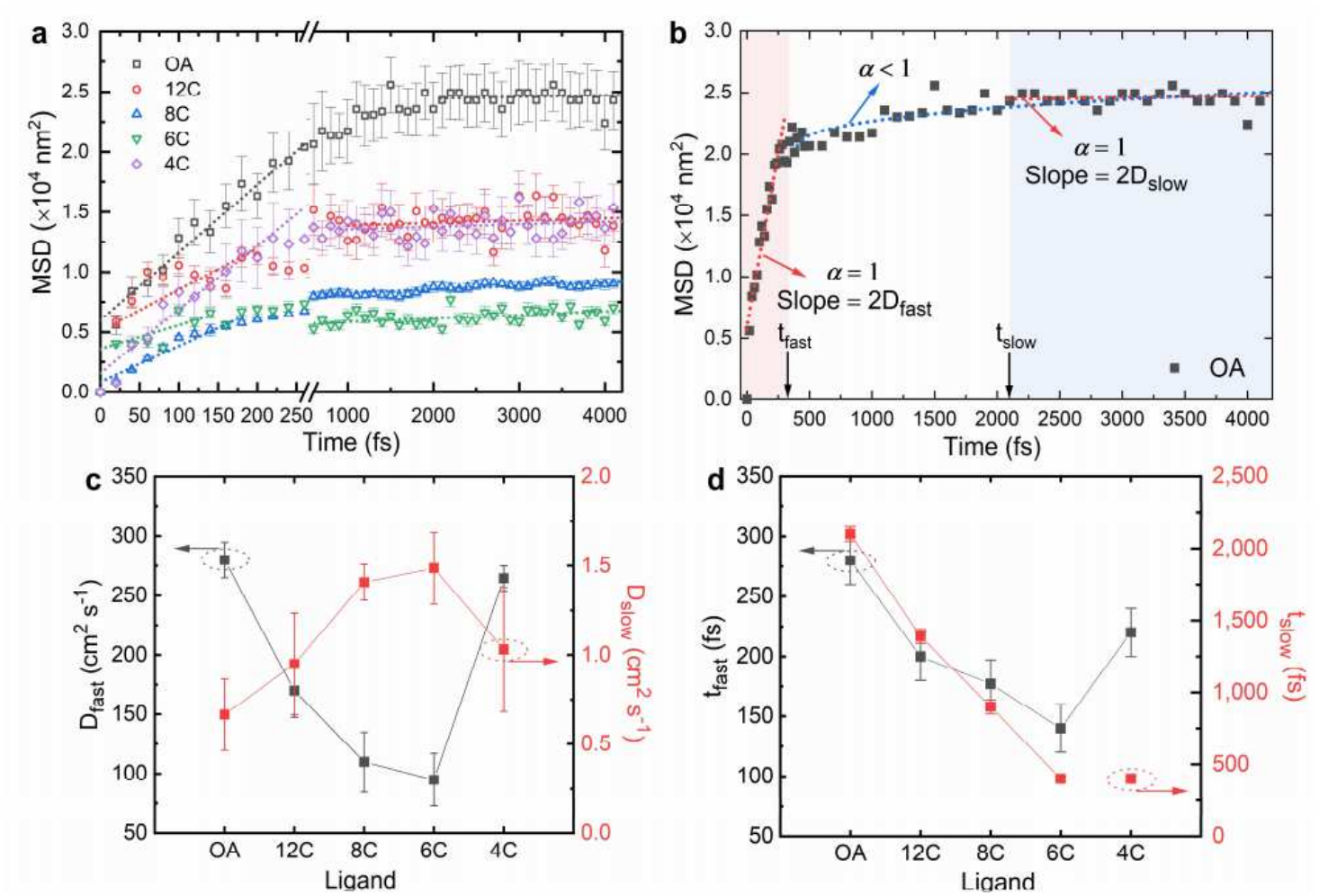


## Figure 2

Quantitative fs-TAM measurement results of the series of QD thin films. a, Time evolution of the MSD = σt2 − σ 2 profile, while σ 2 represents the width of the spatial exciton distribution near zero pump-probe delay. The dotted lines are the fits within the respective time range based on the power law of MSD = 2Dtα, where α = 1. b, The fitted curves and resultants parameters extracted for a representative QD film, OA as an example. The MSD profile within the time range of 0 < t < tfast and that of t > tslow can be well described by the diffusive motion such that α = 1 from the power law equation (red dotted line), where the diffusivities of Dfast and Dslow can be extracted from the slope of the corresponding fitted lines. The MSD profile after tfast can also be described by a subdiffusive motion (blue dotted line, α < 1), while conclusions from the two fitting methods are consistent (Supplementary Discussion 2). c, The extracted diffusivities of the initial fast transport regime (Dfast) and the slow regime (Dslow) of the series of QD films. The two transport regimes show opposite response to the variation of ligands. d, The estimated time duration of the initial fast stage (tfast) and the time taken (from 0 fs) for the excitons to enter the slow transport regime (tslow).

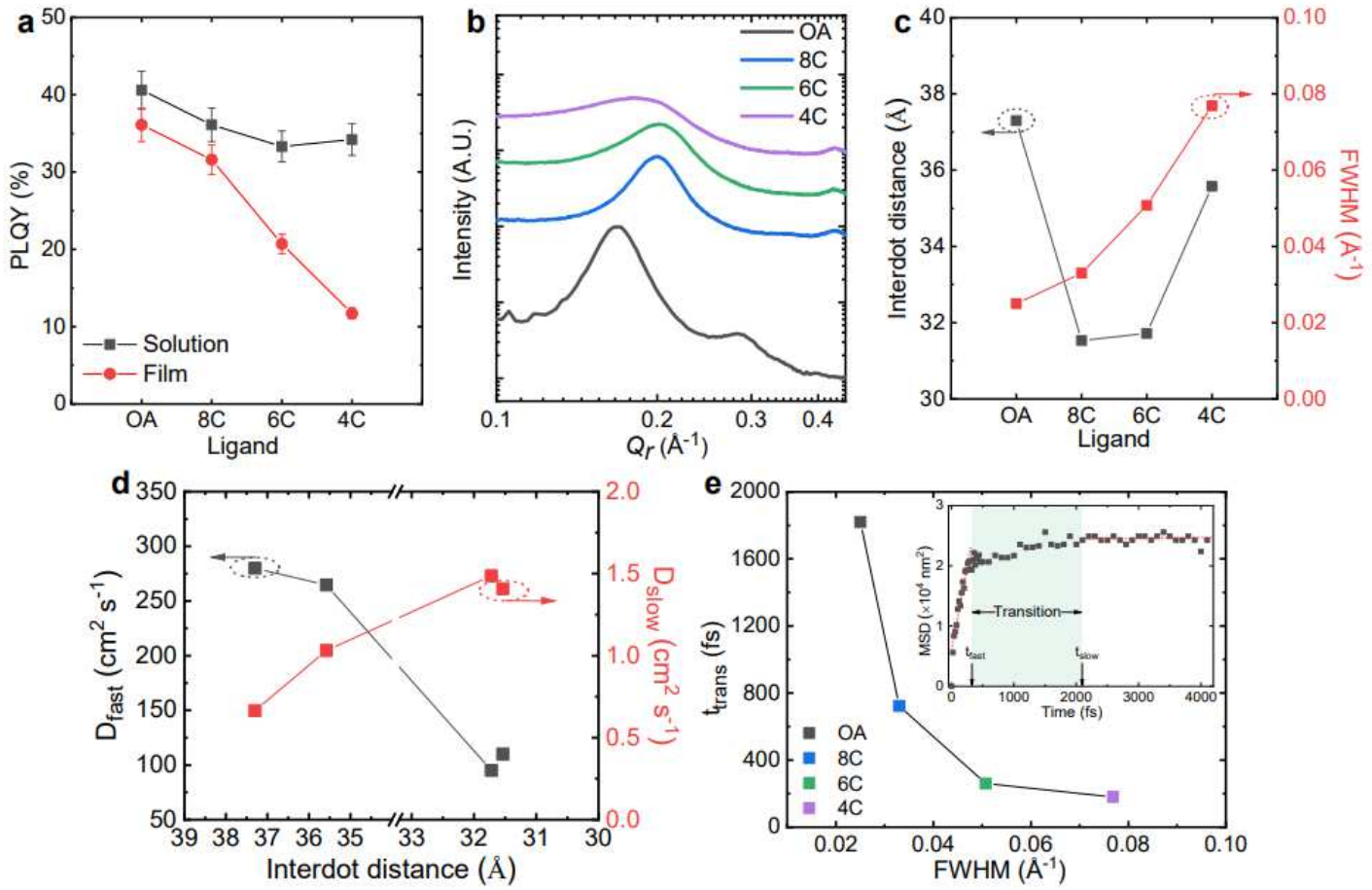


## Figure 3

Quality and structural information of the QDs and films with different ligands and correlation to the fs-TAM results. a, PLQY of the QDs in both solution- and solid- state with different ligands. A more significant quenching in the PLQY can be observed from films with shorter ligands. No chemical or thermal treatment was applied to the films, indicating that the quenching of PLQY arises from improved QD coupling due to closer interdot distance. b, Radially integrated GISAXS intensities of QD solids (normalized). Lower Qr value of the 1st order scattering peaks indicates larger average separation between the QDs, while the peak width indicates discrepancy of the separation. c, The fitted interdot distance and FWHM of the 1st order scattering peaks from b. We ascribe the FWHM to a relative deviation in the core-to-core spacing of the QDs and hence level of packing disorder in the samples. d, Correlation between the actual interdot distance (core-to-core) with the diffusivities of the fast and slow regimes. The Dfast decreases with reducing interdot distance while Dslow clearly shows an opposite trend. e, Correlation between the transition time (ttrans = tslow – tfast, inset) with the FWHM (level of packing disorder) of the 1st order scattering peaks in b. The decreasing ttrans with increasing FWHM indicates higher level of disorder leads to faster transition from the fast to the slow regime.

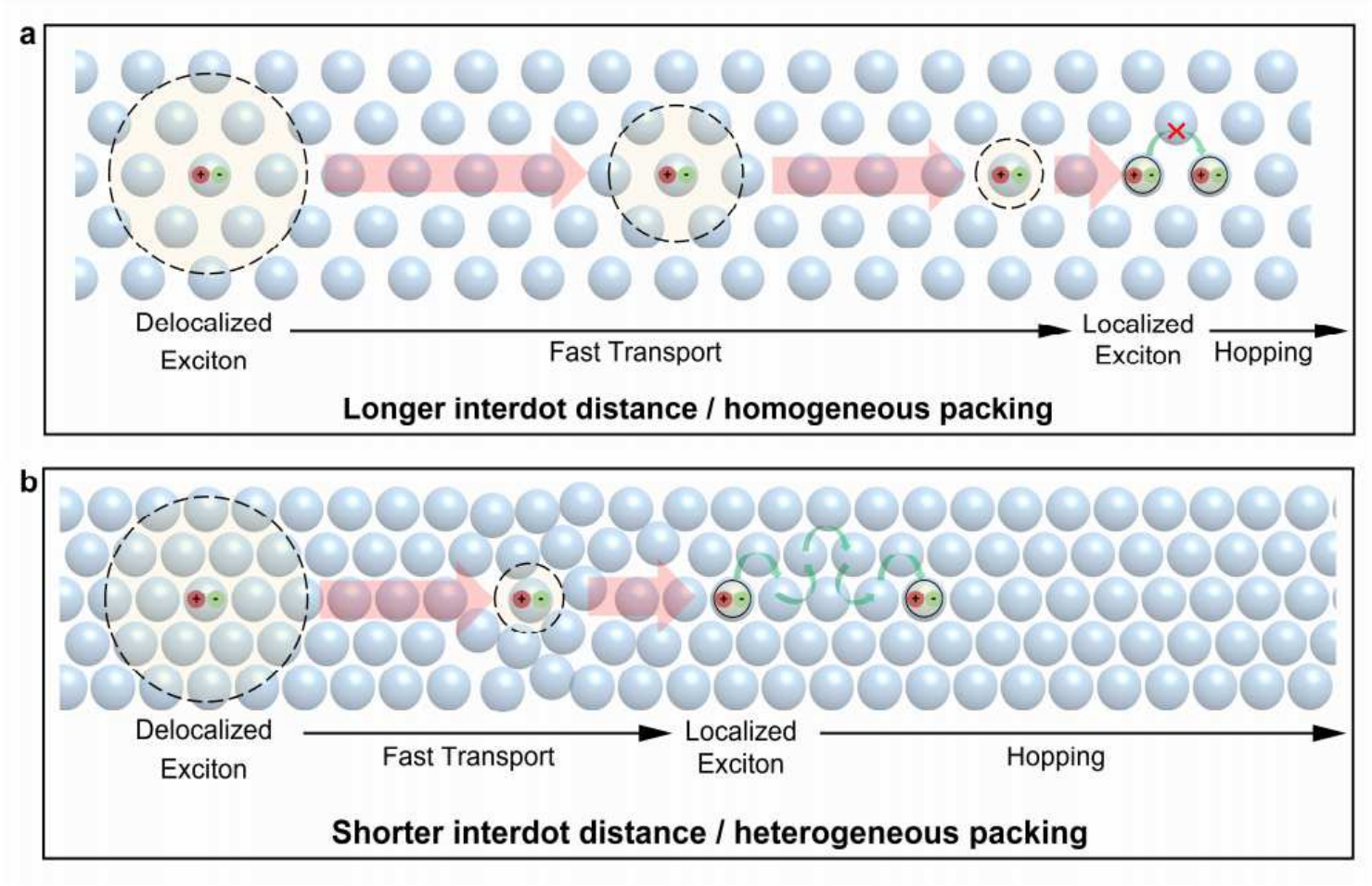


**Figure 4**

Schematic of early time exciton transport in QD solids. a, The case of QD solids with relatively long (but still closely-packed) interdot distance and/or homogeneous packing. The photogenerated exciton initially delocalizes over multiple QDs and diffuses through the QD solid rapidly. The low QD packing density and lack of disorder allows the transport to be faster and sustained longer. As disorders still exist the exciton would eventually be localized, and after the exciton hopping process is inefficient due to the long interdot distance. b, The case of QD solids with shorter interdot distance and/or heterogeneous packing. Due to high QD packing density and the existence of packing disorder, the delocalized exciton diffuses relatively slowly and can be localized much earlier. However, after localization the exciton can keep moving among QDs through hopping due to the shorter interdot distance.

## Supplementary Files

This is a list of supplementary files associated with this preprint. Click to download.

- SupplementaryInformationQDultrafastsubmission.pdf